applied sciences

MDPI

Article

Self-Coherent 448 Gb/s PDM-Twin-SSB PAM-4 Transmission over 80 km SSMF via a Stokes Vector KK Receiver

Xiaoling Zhang [1], Fengying Lu [1], Wensheng Qiao [1] and Yong Geng [2,*]

[1] National Key Laboratory of Complex Aviation System Simulation, Southwest China Institute of Electronic Technology, Chengdu 610036, China
[2] Key Lab of Optical Fiber Sensing and Communication Networks, University of Electronic Science and Technology of China, Chengdu 611731, China
* Correspondence: gengyong@uestc.edu.cn

Abstract

We propose and numerically investigate a four-dimensional (4-D) multiplexed polarization division multiplexing twin single-sideband (PDM-Twin-SSB) PAM-4 transmission scheme enabled by a Stokes vector Kramers–Kronig (SV-KK) receiver, targeting high-capacity short-reach optical interconnects with low-cost implementation. At the transmitter, the PDM-Twin-SSB signal, composed of four independent optical SSB sub-channels, is efficiently generated using two low-cost dual-drive Mach–Zehnder modulators (DDMZMs) driven by a single laser, eliminating the need for multiple laser sources and complex optical filtering. At the receiver, a Stokes vector receiver (SVR) is employed to simultaneously detect the left and right sidebands from both polarizations. Polarization de-rotation, which is essential for recovering the multiplexed signals, is performed directly in the Stokes space. Furthermore, Kramers–Kronig (KK) processing is applied after polarization alignment to reconstruct the complex optical field and mitigate the signal-to-signal beating interference (SSBI) inherent in square-law direct detection. We demonstrate that the 448 Gb/s PDM-Twin-SSB PAM-4 signal can be successfully transmitted over 80 km standard single-mode fiber (SSMF) with a pre-FEC bit-error-rate (BER) below the 7% hard-decision forward error correction (HD-FEC) threshold of 3.8×10^{-3}, achieving an OSNR requirement of 41 dB. The system performance is systematically evaluated through optimization of the carrier-to-signal power ratio (CSPR) and the guard band between the optical carrier and the sidebands. The results confirm that the proposed DDMZM-based PDM-Twin-SSB architecture, combined with the SV-KK receiver, provides a practical and cost-effective polarization-demultiplexing solution for single-wavelength high-speed optical interconnects, enabling robust transmission performance without requiring a local oscillator or active polarization control.

Keywords: stokes vector receiver; Kramers–Kronig; self-coherent; twin single-sideband

Check for updates

Academic Editor: John Xiupu Zhang

Received: 24 September 2026
Revised: 25 October 2026
Accepted: 4 November 2026
Published: 6 November 2026

Copyright: © 2026 by the authors. Licensee MDPI, Basel, Switzerland. This article is an open access article distributed under the terms and conditions of the Creative Commons Attribution (CC BY) license.

1. Introduction

The relentless proliferation of big data, cloud computing, virtual reality, AI-driven services, and the Internet of Things (IoT) continues to drive an unprecedented surge in global Internet traffic [1,2]. Industry forecasts project that global data-center IP traffic will surpass 20 zettabytes (ZB) annually by 2030, propelled by cloud computing, AI workloads, and edge processing [3]. This growth trajectory is being fundamentally reshaped by the rapid adoption of newly developed applications. Cisco projects that AI-related network traffic will triple over the next three years, with inference flows emerging as the dominant driver [4]. To accommodate this insatiable bandwidth demand, substantial research efforts

have been devoted to developing optical transceivers capable of supporting beyond 400 Gb/s per wavelength for short-reach applications. Various advanced modulation formats have been explored to enhance spectral efficiency (SE) in such systems, including carrier-less amplitude–phase modulation (CAP) [5], quadrature amplitude modulation (QAM) [6,7], orthogonal frequency-division multiplexing (OFDM) [8,9], discrete multi-tone (DMT) [10], and pulse amplitude modulation (PAM) [11–13]. Among these, four-level pulse amplitude modulation (PAM-4) has emerged as a particularly attractive candidate, offering the lowest optical power penalty and a straightforward implementation path for single-laser 100G short-reach links relative to more complex modulation schemes.

Meanwhile, wavelength-division multiplexing (WDM) systems have been extensively investigated as a straightforward means of increasing transmission capacity. However, such systems entail considerable cost penalties arising from actively cooled lasers, high power consumption, and complex digital signal processing (DSP) at the receiver, rendering them less attractive for cost-sensitive short-reach applications. Conversely, achieving beyond 400 Gb/s per wavelength using a single laser carrier with intensity modulation and direct detection (IM/DD) remains a substantial challenge [14–16].

In IM/DD systems, single-sideband (SSB) transmission has recently regained significant attention, owing to its inherent resilience to chromatic-dispersion (CD)-induced power fading and its ability to reduce optical spectral occupancy by half. Nevertheless, conventional SSB transmission forfeits half of the digital-to-analog converter (DAC) bandwidth, thereby limiting the achievable system throughput. To fully exploit the available device bandwidth and enhance system capacity, the twin-SSB transmission scheme has been proposed, which simultaneously transmits two independent SSB signals located on both sides of the optical carrier [17–19].

Parallel to these advances in modulation formats, the evolution of sophisticated DSP techniques has created new opportunities for IM/DD systems. In particular, the Kramers–Kronig (KK) coherent receiver enables the reconstruction of the complex optical field from the detected intensity, thereby facilitating linearization of the received signal and compensation of linear impairments [20–27]. When combined with KK processing, polarization division multiplexing (PDM) transmission becomes feasible with a well polarization-aligned local oscillator (LO). Although the PDM-KK system effectively doubles the system capacity, the requirement for both an LO and an active polarization controller remains undesirable for low-cost short-reach applications. Fortunately, the Stokes vector receiver (SVR) offers a compelling alternative, capable of performing polarization demultiplexing directly in the Stokes space without the need for active polarization control or a dedicated LO [27], thus providing a promising pathway toward high-capacity, low-complexity IM/DD systems. Compared with the previous Stokes-vector KK scheme in [25], this work makes three specific contributions as presented in Table 1. First, it extends the multiplexing dimensionality from two sub-channels to four sub-channels by combining two sidebands and two polarizations, i.e., 2 sidebands × 2 polarizations. Second, the twin-SSB signal is generated by two low-cost DDMZMs driven by a single laser, avoiding multiple laser sources and complex optical filtering. Third, polarization de-rotation is performed directly in Stokes space, followed by KK field reconstruction and a low-complexity MIMO equalizer, eliminating the need for a local oscillator and active polarization control.

In this paper, we propose and numerically investigate a self-coherent single-wavelength PDM-Twin-SSB transmission system enabled by a Stokes vector Kramers–Kronig (SV-KK) receiver, which achieves 4-D multiplexed PAM-4 transmission over four independent dimensions, namely the two orthogonal polarizations and the two sidebands, with each dimension carrying an independent PAM-4 signal, while maintaining low hardware complexity. At the transmitter, four independent PAM-4 signals are modulated onto two twin-SSB sub-bands,

which are then mapped onto the two orthogonal polarizations. This is accomplished using two low-cost dual-drive Mach–Zehnder modulators (DDMZMs), which feature simplified bias control. At the receiver, the left sideband (LSB) and right sideband (RSB) of the incoming optical signal are first extracted by two optical band-pass filters (OBPFs). Subsequently, the LSB and RSB components from both polarizations are routed into two separate Stokes vector receivers (SVRs). In the digital domain, polarization de-rotation is performed directly in the Stokes space, followed by Kramers–Kronig (KK) reconstruction to effectively suppress signal-to-signal beating interference (SSBI), thereby enabling linear recovery of the optical field without the need for a local oscillator. In addition, the carrier-to-signal power ratio (CSPR) and the guard band between the optical carrier and the sidebands are optimized. The obtained results substantiate that the proposed self-coherent SV-KK scheme constitutes an effective and cost-efficient polarization-demultiplexing solution for single-wavelength PDM-Twin-SSB systems, underscoring its promising potential as a competitive candidate for next-generation high-speed short-reach optical interconnects.

Table 1. Comparison with the previous Stokes-vector KK transmission.

Feature	Ref. [25]	This Work
Transmission format	PDM single-SSB	PDM-Twin-SSB
Multiplexing dimension	2 sidebands × 1 polarization	2 sidebands × 2 polarizations (4-D)
Sub-channels	2	4
Modulator type	IQ/DPMZM	2 × DDMZM
Carrier	Digital	Optical
DAC-ENoB & dynamic range	High	Low

2. Principle

PDM transceivers have been extensively deployed in optical coherent communication systems, wherein the received signal is fully recoverable in Jones space via 2 × 2 multiple-input multiple-output (MIMO) equalization. The Jones space constitutes a two-dimensional complex vector space, in which each dimension represents an orthogonal state of polarization (SOP) endowed with both amplitude and phase information. Such a representation enables coherent receivers to accomplish simultaneous field reconstruction and polarization demultiplexing. In PDM IM/DD systems, however, polarization recovery presents a substantially greater challenge, owing to the complete absence of phase information, as depicted in Figure 1a. The Stokes space, in contrast, furnishes a three-dimensional real-valued representation, wherein each dimension corresponds to the optical power difference subsequent to the field traversing distinct pairs of orthogonal polarizers. This intrinsic property renders the Stokes space particularly well-suited for polarization demultiplexing in IM/DD systems, circumventing the need for explicit phase retrieval. The Stokes vector of the optical field is defined as

$$\begin{bmatrix} S_0 \\ S_1 \\ S_2 \\ S_3 \end{bmatrix} = \begin{bmatrix} |X|^2 + |Y|^2 \\ |X|^2 - |Y|^2 \\ 2\mathrm{Re}\{XY^*\} \\ 2\mathrm{Im}\{XY^*\} \end{bmatrix} \quad (1)$$

where $\mathrm{Re}\{\cdot\}$ and $\mathrm{Im}\{\cdot\}$ represent the real and imaginary parts of the complex electric-field components, respectively. The first Stokes parameter, S_1 quantifies the optical power differential following projection onto orthogonal linear polarizers oriented along the X and Y axes. The second parameter, S_2 represents the analogous power difference subsequent to polarizers aligned at +45° and −45°, whereas the third parameter, S_3 is derived from the

differential power measured after right-hand and left-hand circular polarizers. In addition, the parameter $S_0 = \sqrt{S_1^2 + S_2^2 + S_3^2}$ defined as the total optical power across both X and Y polarizations, which is often employed to give a 4-D Stokes vector for Stokes-space field visualization. With Stokes vector, the 2-D complex-valued Jones vector is mapped into the 4-D real-valued Stokes vector. By simply combing the S_0 and S_1, we can regenerate the intensity of X polarization, $(S_0 + S_1)/2$, and Y polarization, $(S_0 - S_1)/2$.

Figure 1b depicts a modified SVR architecture incorporating two single-ended photodiodes (PDs) and two balanced photodetectors (BPDs). A polarization beam splitter (PBS) first decomposes the incoming polarization-multiplexed signal into two orthogonal SOPs, each of which is subsequently bifurcated into two equal branches. One branch from each polarization is routed to a single-ended PD for direct intensity detection of the X and Y polarizations, whereas the remaining branches are combined through a 90° optical hybrid, with one path undergoing a 90° polarization rotation to ensure that the interfering fields within the hybrid share an identical polarization basis. The output signals of the optical hybrid are then detected by the two BPDs.

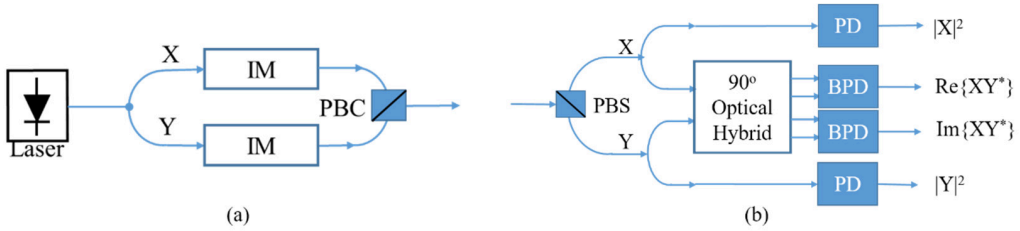


Figure 1. (**a**) Polarization-multiplexed intensity modulation. (**b**) Modified SVR with two PDs and two BPDs.

After optical fiber transmission, the SOP of the optical field undergoes a rotation, thereby inducing polarization crosstalk between the two orthogonal channels. A 4 × 4 real-valued MIMO equalizer is employed to estimate the polarization de-rotation matrix, followed by KK processing for field reconstruction. It should be noted, however, that the MIMO-based approach necessitates training symbols for polarization estimation. An alternative strategy circumvents this requirement by performing polarization de-rotation directly in the Stokes space, exploiting the statistical distribution of the received signals. The received Stokes vectors are uniquely characterized by a symmetry plane with normal vector $\mathbf{n} = (n_1, n_2, n_3)$, which can be determined via a least-squares fit of the measured Stokes vectors. In the Poincaré sphere representation, all such vectors reside on the plane X = 0 with normal is $(1, 0, 0)$. The corresponding transformation matrix in Stokes space is consequently expressed as,

$$TM = \begin{bmatrix} \cos(\theta) & -\sin(\theta) & 0 \\ \sin(\theta)\cos(\Delta\phi) & \cos(\theta)\cos(\Delta\phi) & -\sin(\Delta\phi) \\ \sin(\theta)\sin(\Delta\phi) & \cos(\theta)\sin(\Delta\phi) & -\cos(\Delta\phi) \end{bmatrix} \quad (2)$$

where $\theta = \arctan(\sqrt{n_2^2 + n_3^2}, n_1)$ represents the polarization rotation angle, and $\Delta\phi = \arctan(n_3, n_2)$ denotes the phase delay between the two orthogonal polarization modes. The tracking and correction of the state of polarization (SOP) is accomplished by multiplying the inverse of the transformation matrix with the received Stokes vectors, $TM^{-1}[S_1, S_2, S_3]^T$, thereby restoring the polarization alignment without requiring active polarization control.

3. System Setup and DSP

We evaluate the performance of the proposed PDM-Twin-SSB PAM-4 transmission system using Virtual Photonics Incorporated Transmission Maker (VPI TM 9.0, manufactured

by VPIphotonics GmbH, Berlin, Germany) with co-simulations of Matlab (R2015b). The setup of the SVR-based PDM-Twin-SSB system is depicted in Figure 2a. Two DDMZMs are employed to generate the PDM-Twin-SSB signal. The driving signal $S_{x(y),r(l)}$ corresponds to the RSB or LSB component in the X or Y polarization, respectively, while $\hat{S}_{x(y),r(l)}$ denotes its corresponding Hilbert transform. For each polarization, two independent PAM-4 driving signals are combined to drive the upper arm of the DDMZM, whereas their Hilbert-transformed counterparts are subtracted to drive the lower arm, thereby generating the twin-SSB signal. Both DDMZMs are biased at the quadrature point to ensure linear modulation. The two generated twin-SSB signals are then combined via a polarization beam combiner (PBC) and launched into the fiber link.

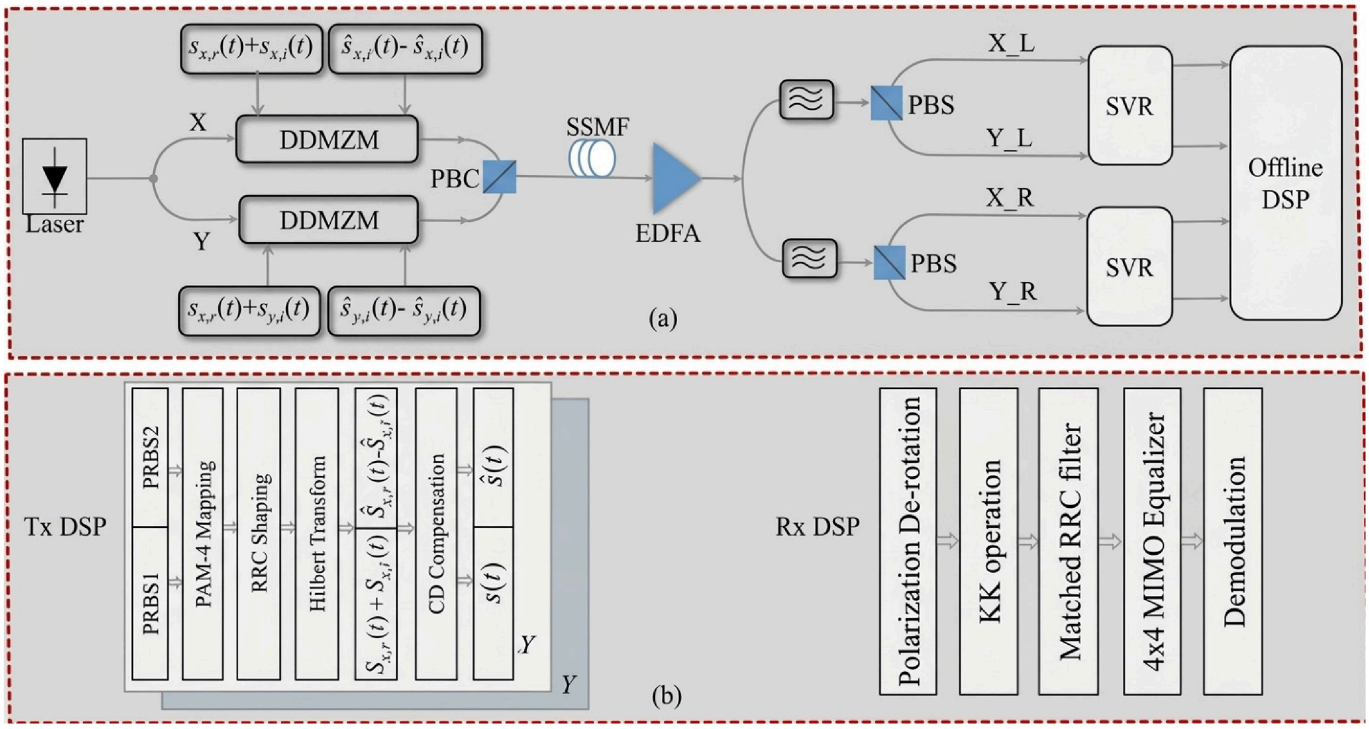


Figure 2. (**a**) System setup. (**b**) Transceiver DSP.

At the receiver (Rx) side the optical signal is first amplified by an erbium-doped fiber amplifier (EDFA) to compensate for the fiber loss. Subsequently, two optical band-pass filters (OBPFs) are employed to extract the LSB and RSB components from both polarizations, corresponding to X_L, Y_L, X_R and Y_R, respectively. The LSB pair (X_L and Y_L) and the RSB pair (X_R and Y_R) are then routed into two separate SVRs, each configured as described in Figure 1b. Finally, the detected signals from both SVRs are processed by the receiver DSP for subsequent polarization de-rotation and signal recovery. The fiber link, optical filters, SVR, and DSP are modeled according to the parameters listed in Table 2. The laser is modeled as a continuous-wave source with a linewidth of 100 kHz at 1550 nm. The 80 km SSMF link is modeled with an attenuation of 0.2 dB/km, a dispersion of 16 ps/nm/km, and a dispersion slope of 0.08 ps/(nm^2·km). The EDFA is used to compensate for fiber loss, and its noise figure is set to 5 dB.

The digital signal processing (DSP) chain of the transceiver is depicted in Figure 2b. The twin-SSB generation procedure is identical for both orthogonal polarization states; hence, the X polarization is taken as a representative example. Two independent pseudo-random bit sequences (PRBSs) with length of $2^{15} - 1$ are first generated for PAM-4 modulation, then up-sampled by a factor of 2 and shaped by a root-raised cosine (RRC) Nyquist filter with a roll-off factor of 0.01. Then, the generated Nyquist PAM-4 signals $S_{x,r}(t)$ and $S_{x,l}(t)$

are combined to drive the upper arm of the modulator, whereas their Hilbert pairs $\hat{S}_{x,r}(t)$ and $\hat{S}_{x,I}(t)$ are subtracted to drive the lower arm, thereby synthesizing the twin-SSB optical signal $E_{out} = E_{in}\left[1 - j + \left(S_{x,r}(t) + j\hat{S}_{x,r}(t)\right) + \left(S_{x,I}(t) - j\hat{S}_{x,I}(t)\right)\right]$. In the DDMZM-based twin-SSB generation, the upper and lower arms are driven by s(t) and its Hilbert transform ŝ(t), respectively. With the modulator biased at the quadrature point and under the small-signal approximation, the output field can be written as $E_{out}(t) \approx 1 - j + \left(S(t) + j\hat{S}(t)\right) + \left(\hat{S}(t) - jS(t)\right)$, so that the DC carrier term naturally takes the form $1 - j$, reflecting the quadrature bias and the 90° phase relation between the two arms. The CSPR is calculated by spectral integration of the optical carrier and the SSB components, and the guard band is defined as the frequency spacing between the optical carrier and the edge of each SSB sub-channel. All key parameters and DSP settings are summarized in Table 2 to facilitate reproduction. At the receiver side, the signal is first amplified by the EDFA and then split into the LSB and RSB paths by two fourth-order Gaussian OBPFs. The LSB pair and the RSB pair are detected by two separate SVRs. Each SVR consists of a PBS, two single-ended PDs, a 90° optical hybrid, and two BPDs, as shown in Figure 1b. The PD responsivity and thermal noise are set to 0.8 A/W and 21 pA/√Hz in the simulation. The received LSB and RSB signals are first mapped into the Stokes space for polarization de-rotation. The recovered Stokes vectors corresponding to the two sidebands in each polarization are then utilized to retrieve the original PAM-4 signals. Since SSB signal detection relies on direct optical power measurement, the square-law operation of the photodiode (PD) inevitably introduces signal-to-signal beating interference (SSBI) [28,29]. To mitigate this impairment, a Kramers–Kronig (KK) receiver with up-sampled by a factor of 2 is employed to reconstruct the complex optical field after polarization de-rotation, thereby linearizing the received signal. Subsequently, a matched filter is applied for PAM-4 signal recovery. Finally, the four recovered PAM-4 signals are processed by a MIMO equalizer employs a decision-directed LMS algorithm with 1024 training symbols to suppress residual polarization crosstalk and linear inter-symbol interference between the twin-SSB sub-bands. A fourth-order Gaussian OBPF is used, with its passband width individually optimized for each guard band. Table 2 summarizes the principal parameters adopted in the system.

Table 2. The system parameter.

Parameter	Value	Parameter	Value
Laser power	10 dBm	Fiber length	80 km
Laser linewidth	100 kHz	Fiber attenuation	0.2 dB/km
Laser wavelength	1550 nm	Fiber dispersion	16 ps/nm/km (typical G.652.D)
Total baud rate	4 × 56 Gbaud	Fiber dispersion slope	0.08 ps/(nm^2 km) (typical G.652.D)
Launch optical power	5 dBm	Modulator extinction ratio	30 dB
Modulator insertion loss	6 dB	Gaussian OBPF order	4

4. Discussion

Figure 3 depicts the output optical spectrum of the DDMZM for the X polarization, where the LSB and RSB are symmetrically positioned on both sides of the optical carrier with a designated guard band. The Y polarization exhibits an identical spectral distribution. The CSPR, defined as the ratio of the optical carrier power to that of the SSB signals, is derived from the twin-SSB optical spectrum via spectral integration of the respective power components. Subsequently, the CSPR is optimized by adjusting the driving amplitude applied to the DDMZM.

Figure 4 presents the bit-error-rate (BER) performance as a function of CSPR under various guard band configurations, evaluated for both back-to-back (B2B) and 80 km

standard single-mode fiber (SSMF) transmission scenarios. The optical signal-to-noise ratio (OSNR) is fixed at 40 dB for the B2B case and 42 dB for the 80 km SSMF case, respectively. In the numerical simulation, a fourth-order Gaussian optical band-pass filter (OBPF) is adopted, with its passband width individually optimized for each guard band to suppress inter-channel crosstalk. As the guard band narrows, the optimal CSPR increases, owing to the reduced spectral distance to the carrier and the penalty imposed by laser linewidth.

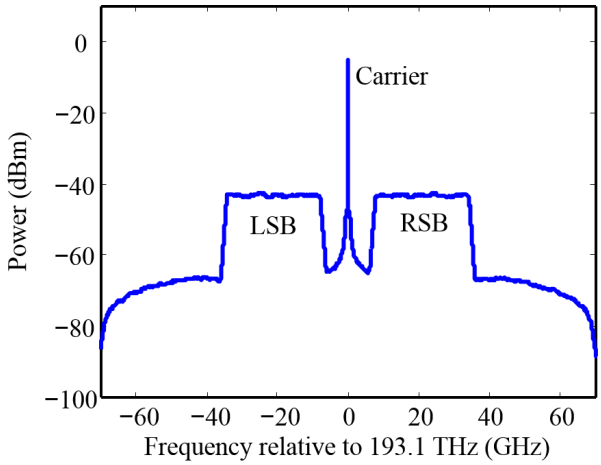


Figure 3. Optical spectrum of the DDMZM of X polarization.

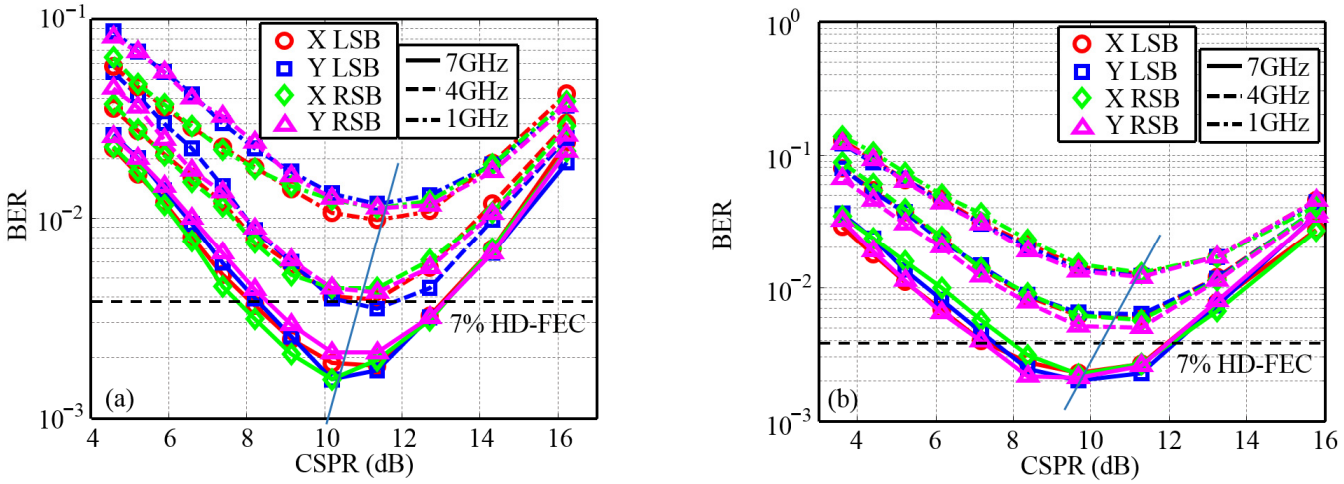


Figure 4. The BER performance versus CSPR with different guard bands. (**a**) B2B. (**b**) 80 km SSMF.

Beyond the optimization of the CSPR for SSB signal detection, the impact of the guard band separating the SSB signal from the optical carrier is systematically examined in Figure 5a. A guard band of 2 GHz is observed to yield a pre-FEC BER below the 7% hard-decision forward error correction (HD-FEC) threshold (3.8×10^{-3}) for 80 km SSMF transmission. To ensure a more robust performance margin, a guard band of 7 GHz is selected for all subsequent investigations. With the guard band fixed, the CSPR is further optimized under varying OSNR regimes, with the results presented in Figure 5b. The optimal CSPR reveals a strictly monotonic dependence on OSNR, increasing progressively as the OSNR improves. This behavior is inherent to the DDMZM-based SSB modulation architecture, where the optical carrier power remains constant, while the signal amplitude can be decreased in response to superior signal quality, thereby yielding a higher optimal CSPR. Following this parametric optimization, the transmission performance as a function of OSNR is evaluated, and the corresponding outcomes are illustrated in Figure 5c. With

the assistance of the SVR, the 448 Gb/s PDM-Twin-SSB PAM-4 system reaches a pre-FEC BER of 3.8×10^{-3} at an OSNR of 39 dB for the B2B configuration and 41 dB for the 80 km SSMF link.

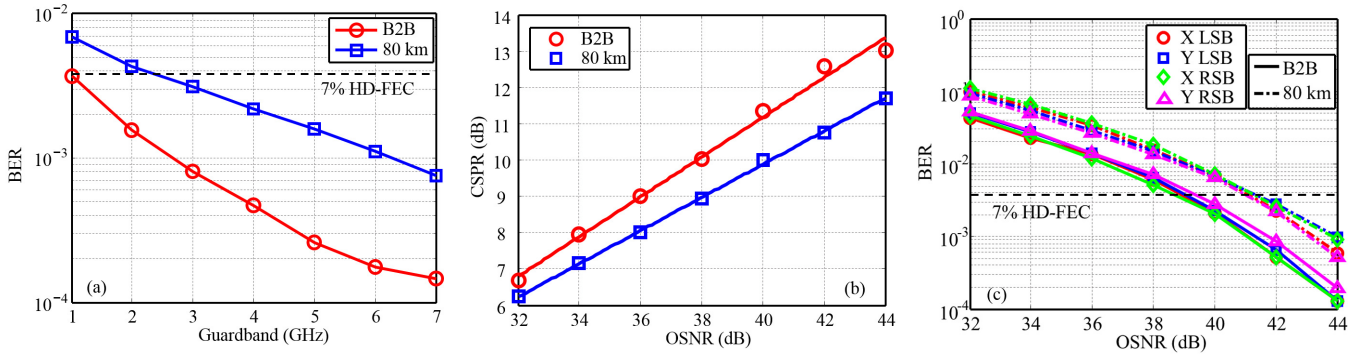


Figure 5. (**a**) The BER versus guard band. (**b**) The optimal CSPR versus the OSNR with 7 GHz guard band. (**c**) The system performance with different OSNR.

The BER performance across the four independent sidebands remains consistent, owing to the joint application of SVR-based polarization de-rotation and a subsequent MIMO equalizer. Figure 6a displays the distribution of the received Stokes vectors (SVs) on the Poincaré sphere, represented by the coordinates (S_1, S_2, S_3). A 3 × 3 rotation matrix (RM) is computed from the normal vector of the least- LSP) fitted to the received SVs, and is then applied to perform polarization de-rotation. Following multiplication by the inverse of the RM, the SVs become well concentrated and aligned, as illustrated in Figure 6b, confirming the effectiveness of the Stokes-space polarization demultiplexing procedure.

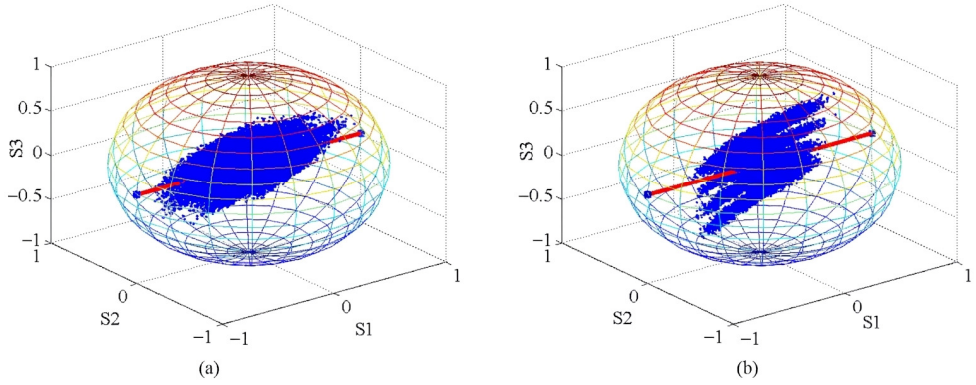


Figure 6. Received Stokes vectors in Poincare sphere with PAM-4 modulation after 80 km SSMF. (**a**) Before polarization de-multiplexing. (**b**) After polarization de-multiplexing.

Upon polarization de-rotation, the optical powers of the two orthogonal polarizations are retrieved from S_0 and S_1. Owing to system noise, however, the accuracy of the rotation matrix (RM) estimation in Stokes space is inevitably degraded. Consequently, subsequent to polarization de-rotation and Kramers–Kronig (KK) processing, a 4 × 4 MIMO equalizer is employed to mitigate residual polarization crosstalk and linear interference. For comparison, the system performance without SVR—i.e., relying solely on the 4 × 4 MIMO DSP is also assessed Figure 7a compares the BER performance of different polarization de-rotation DSP schemes over 80 km transmission. The cascaded SVR and 13-tap MIMO DSP yields the best performance. In contrast, in the absence of SVR, the system fails to reach the 7% HD-FEC threshold with the same tap count, as the polarization crosstalk remains insufficiently compensated. Furthermore, it suffers from an approximately 2 dB OSNR penalty even

when a 51-tap MIMO equalizer is employed. To elucidate the underlying mechanism behind this performance discrepancy, the LSB of the X polarization is taken as a representative example. The four taps are c10, c11, c12, and c13, correspond to the LSB of the X and Y polarizations and the RSB of the X and Y polarizations, respectively. The corresponding tap coefficients are plotted in Figure 7b,c. Tap c11 serves to mitigate residual polarization interference. Since the SVR aligns the signal polarization, the c11 coefficient in the absence of SVR exhibits two pronounced peaks that are larger than those observed with SVR. The values of c12 and c13 remain near zero, as the RSB is eliminated by the OBPF. It is worth noting that the taps of the 4 × 4 MIMO DSP for each sideband exhibit similar distributions.

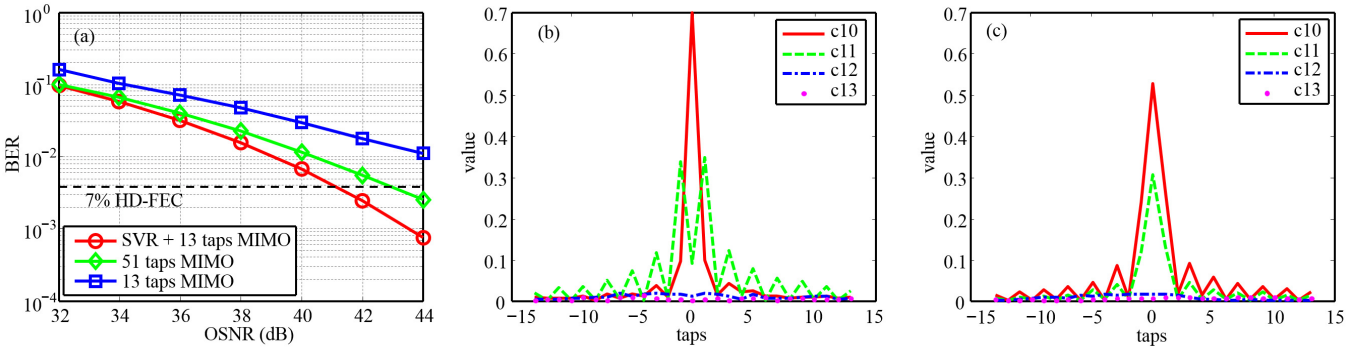


Figure 7. (**a**) The BER performance with different receiver polarization de-rotation DSP. (**b**) The taps coefficient of the MIMO equalizer without SVR. (**c**) The taps coefficient of the MIMO equalizer with SVR.

The proposed scheme simplifies polarization recovery to a 3 × 3 real-valued matrix operation, compared with the 2 × 2 complex MIMO (equivalent to 4 × 4 real MIMO) in standard coherent receivers., the complexity advantage of this paper lies primarily at the hardware level (no LO, no active polarization control) and DSP multiplications. The comparison is presented at Table 3.

Table 3. Two scheme comparison.

Item	Standard Coherent MIMO Receiver	Proposed SV-KK Receiver
Local oscillator	Required	Not required
90° optical hybrid	Required	Required
Balanced PDs	Required (×4)	Required (×4)
Active polarization control	Required	Not required
ADC channels	4	4
Receiver	51taps	SVR + 13taps

5. Conclusions

In this paper, we have numerically demonstrate a single-wavelength PDM-Twin-SSB PAM-4 transmission system based on an SV-KK receiver. The scheme uses only two DDMZMs and a single laser to achieve a 448 Gb/s four-dimensional multiplexed transmission over 80 km of SSMF. By performing polarization de-rotation directly in the Stokes space, the proposed scheme substantially reduces receiver complexity compared to conventional MIMO-based polarization demultiplexing approaches. We have also conducted a comprehensive optimization of the CSPR and the guard band between the optical carrier and the sidebands, identifying optimal operating conditions for both back-to-back and 80 km SSMF transmission scenarios. The results demonstrate that the 448 Gb/s PDM-Twin-SSB PAM-4 signal can achieve pre-FEC BER performance below the 7% HD-FEC threshold,

validating the feasibility of the proposed architecture for high-capacity short-reach interconnects. Importantly, the SV-KK receiver effectively addresses the polarization-demultiplexing challenge without requiring a local oscillator or active polarization control, offering a compelling trade-off among performance, complexity, and cost. These features position the proposed scheme as a competitive candidate for next-generation data-center interconnects and metro-access networks.

Author Contributions: Conceptualization, X.Z. and Y.G.; methodology, X.Z.; validation, X.Z.; formal analysis, Y.G.; investigation, X.Z.; resources, X.Z. and Y.G.; data curation, Y.G.; writing—original draft preparation, X.Z.; writing—review and editing, X.Z., W.Q., F.L. and Y.G.; visualization, F.L. and Y.G.; supervision, W.Q., F.L. and Y.G.; project administration, F.L. and X.Z.; funding acquisition, W.Q. and X.Z. All authors have read and agreed to the published version of the manuscript.

Funding: This work is supported by Southwest Electronic Technology Research Institute Technology Innovation Fund Project (No. H19015) and Development Fund Project of China Electronics Technology Group Corporation (No. R25002).

Institutional Review Board Statement: Not applicable.

Informed Consent Statement: Not applicable.

Data Availability Statement: The data and simulation parameter files supporting this study are available from the corresponding author upon reasonable request.

Conflicts of Interest: The authors declare no conflicts of interest.

References

1. Mordor Intelligence. *Network Router—Market Share Analysis, Industry Trends & Statistics, Growth Forecasts (2026–2031). Hyderabad, India: Mordor Intelligence*; Mordor Intelligence; Hyderabad, India, 2026.
2. Research and Markets. Data Center Interconnect Global Strategic Market Report 2024–2030: Rapid Pace of Digital Transformation Necessitates Robust Data Centers, Drives Opportunities for DCI Solutions. Available online: https://www.globenewswire.com/news-release/2024/04/08/2859018/28124/en/Data-Center-Interconnect-Global-Strategic-Market-Report-2024-2030-Rapid-Pace-of-Digital-Transformation-Necessitates-Robust-Data-Centers-Drives-Opportunities-for-DCI-Solutions.html (accessed on 6 March 2025).
3. IDC (International Data Corporation). Global Data Center IP Traffic Forecast. 2026. Available online: https://www.idc.com (accessed on 1 September 2026).
4. Cisco Systems. Cisco Live 2026 Keynote Address. presented by Chuck Robbins (CEO), Las Vegas, June 2026. Available online: https://newsroom.cisco.com/c/r/newsroom/en/us/a/y2026/m06/cisco-live-2026-keynotes-tldr-edition.html (accessed on 4 June 2026).
5. Wei, J.; Eiselt, N.; Sanchez, C.; Du, R.; Griesser, H. 56 Gb/s multi-band CAP for data center interconnects up to an 80 km SMF. *Opt. Lett.* **2016**, *41*, 4122–4125. [CrossRef]
6. Zhang, L.; Yang, X.; Wang, K.; Wang, C.; Sang, B.; Long, J.; Ding, J.; Zhang, J.; Zhu, M.; Yu, J. Real-time 60 Gb/s PS-64QAM SSB-DMT transceiver deploying a low-complexity distribution matcher in band-limited IM-DD system. *Opt. Fiber Technol.* **2025**, *89*, 104048. [CrossRef]
7. Gan, X.; Xiang, M.; Xu, J.; Zhou, G.; Fu, S.; Qin, Y. Carrier-free phase retrieval of dual-polarization QAM signals aided by polarization rotation estimation. *Opt. Express* **2026**, *34*, 3153. [CrossRef]
8. Liu, Y.; Chen, M.; Gao, X.; Cheng, Y. Symbol-interleaved precoding technique for DDO-OFDM systems with the KK receiver. *Opt. Express* **2022**, *30*, 43633. [CrossRef]
9. Chen, M.; Zhang, L.; Xi, D.; Liu, G.; Zhou, H.; Chen, Q. Experimental demonstration of DFT-precoded guard-band OSSB-OFDM signal reception with ADC undersampling technique. *IEEE Access* **2020**, *8*, 16838–16845. [CrossRef]
10. Chen, M.; Xu, J.; Zhou, J.; Li, H.; Liu, Y. Real-time 30-GSa/s precoded and partial pre-emphasized DMT Transceiver for short-reach IMDD transmission. *J. Lightw. Technol.* **2024**, *42*, 1861–1869. [CrossRef]
11. Zhu, M.; Zhang, J.; Yi, X.; Ying, H.; Li, X.; Luo, M.; Song, Y.; Huang, X.; Qiu, K. Optical single side-band Nyquist PAM-4 transmission using dual-drive MZM modulation and direct detection. *Opt. Express* **2018**, *26*, 6629–6638. [CrossRef]
12. Cao, J.; Wei, H.; Chen, W.; Zhang, H.; Cui, A.; Li, X.; Lu, C.; Lau, A.P.T.; Guo, C.; Zhong, K. Experimental Demonstration of 224 Gbit/s PM-PAM4 IM/DD Transmission System Using TFLN Polarization Controller. *J. Lightw. Technol.* **2025**, *44*, 997–1004. [CrossRef]

13. Zhu, Y.; Fang, X.; Zhang, F.; Hu, W. Direct detection transmission of a PAM signal with power fading mitigation based on Alamouti coding and dual-drive MZM. *Opt. Express* **2022**, *30*, 9321. [CrossRef]
14. Zhang, Z.; Zhu, Y.; Hu, Y.; Hu, W. 400 Gbps/λ transmission based on linear hybrid receiver for Intra-datacenter-interconnects. In Proceedings of the 2025 European Conference on Optical Communications (ECOC), Copenhagen, Denmark, 28 September–2 October 2025.
15. Zhao, Z.; Yang, A.; Huang, X.; Guo, P.; Zhao, S.; Xu, T.; Wan, W.; Bo, T.; Tan, Z.; Dong, Y.; et al. Joint Bandwidth Limitation and Electrical Dispersion Pre-Compensation in Cost-Sensitive IM/DD Transmission Systems. *J. Lightw. Technol.* **2026**, *44*, 34–46. [CrossRef]
16. Yan, A.; Zhao, J.; Li, G.; Luo, P.; Xing, S.; Shen, W.; Hu, Y.; Sun, A.; Shi, J.; He, Z.; et al. Band-interleaving and entropy-loading subcarrier multiplexing modulation for 400G/λ intra-datacenter connections based on hybrid receivers. *J. Lightw. Technol.* **2025**, *43*, 2132–2142. [CrossRef]
17. Wei, Y.; Liu, C.; Sang, B.; Ye, B.; Zhao, F.; Yu, J. Demonstration of 200 Gbit/s Single λ Dual Band DMT Transmission with a SE of 6.29 bit/s/Hz. *J. Lightw. Technol.* **2021**, *39*, 2754–2761. [CrossRef]
18. Li, J.; An, S.H.; Su, Y. Zero-guard band dual-SSB PAM4 signal transmission with joint equalization scheme. *Opt. Lett.* **2020**, *45*, 6178. [CrossRef]
19. Li, X.L.; Xiao, J.; Li, P.C.; Zhao, J.; Chen, J.J.; Chen, L. Low-complexity single-feedback SSBI cancellation for independent dual-SSB direct detection systems. *Opt. Lett.* **2026**, *51*, 3497. [CrossRef]
20. Lowery, A.J.; Feleppa, T. Analog Low-Latency Kramers-Kronig optical Single-Sideband Receiver. *J. Lightw. Technol.* **2021**, *39*, 3130–3136. [CrossRef]
21. Mecozzi, A.; Antonelli, C.; Shtaif, M. Kramers–Kronig coherent receiver. *Optica* **2016**, *3*, 1220–1227. [CrossRef]
22. Szafraniec, B.; Nebendahl, B.; Marshall, T. Polarization demultiplexing in Stokes space. *Opt. Express* **2010**, *18*, 17928–17939. [CrossRef]
23. Che, D.; Shieh, W. Polarization Demultiplexing for Stokes Vector Direct Detection. *J. Lightw. Technol.* **2016**, *34*, 754–760. [CrossRef]
24. Che, D.; Hu, Q.; Shieh, W. Linearization of Direct Detection Optical Channels Using Self-Coherent Subsystems. *J. Lightw. Technol.* **2016**, *34*, 516–524. [CrossRef]
25. Hoang, T.M.; Sowailem, M.Y.S.; Zhuge, Q.; Xing, Z.; Morsy-Osman, M.; El-Fiky, E.; Fan, S.; Xiang, M.; Plant, D.V. Single wavelength 480 Gb/s direct detection over 80 km SSMF enabled by Stokes vector Kramers Kronig transceiver. *Opt. Express* **2017**, *25*, 33534–33542. [CrossRef]
26. Zhang, L.; Yu, J.; Zhu, M.; Zhang, J.; Ma, H.; Cai, Y.; Lei, M.; Chen, X.; Ding, J.; Wang, Y.; et al. Real-time simplified coherent photon-assisted fiber-terahertz integrated system using parallel Kramers–Kronig receiver and FPGA operation. *J. Lightw. Technol.* **2026**, *44*, 1367–1378. [CrossRef]
27. Fang, Y.; Zhu, H.; Cheng, X.; Lu, W.; Yuan, P.; Shi, D.; Lu, D.; Ji, H.; Shieh, W. Cost-effective 228 Gb/s extended-reach SC-PON using a dithered uncooled DFB laser and hybrid-integrated Stokes receiver. *J. Opt. Commun. Netw.* **2026**, *18*, 654–662. [CrossRef]
28. Lu, B.; Liu, X.; Jin, W.; He, J.; Faruk, M.S.; Yi, X.; Gonem, O.F.A.; Wang, B.; Zhang, W.; Giddings, R.; et al. Iterative SSBI mitigation-enabled global linearization of seamlessly converged fiber-mmWave transmission systems. *J. Opt. Commun. Netw.* **2026**, *18*, 915. [CrossRef]
29. Zhang, Y.; Zhu, Y.; Man, L.; Huang, D.; Zhuge, Q.; Hu, W. Low-Complexity Circular-Based SSBI Extraction for 200-Gb/s Direct Detection Transmission With Skew-Enabled VSB Modulation Over 80 km. *J. Lightw. Technol.* **2026**, *44*, 2087–2095. [CrossRef]

Disclaimer/Publisher's Note: The statements, opinions and data contained in all publications are solely those of the individual author(s) and contributor(s) and not of MDPI and/or the editor(s). MDPI and/or the editor(s) disclaim responsibility for any injury to people or property resulting from any ideas, methods, instructions or products referred to in the content.